Title

Millennial-Scale Changes in Terrestrial and Marine Nitrous Oxide Emissions at the Onset and Termination of Marine Isotope Stage 4

Journal

Geophysical Research Letters, 47(22)

ISSN

0094-8276

Authors

Menking, JA
Brook, EJ
Schilt, A
et al.

Publication Date

2020-11-28

DOI

10.1029/2020gl089110

Peer reviewed

AGU ADVANCING EARTH AND SPACE SCIENCE

Geophysical Research Letters

RESEARCH LETTER
10.1029/2020GL089110

Millennial-Scale Changes in Terrestrial and Marine Nitrous Oxide Emissions at the Onset and Termination of Marine Isotope Stage 4

J. A. Menking[1], E. J. Brook[1], A. Schilt[1], S. Shackleton[2], M. Dyonisius[3], J. P. Severinghaus[4], and V. V. Petrenko[3]

[1]College of Earth, Ocean, and Atmospheric Sciences, Oregon State University, Corvallis, OR, USA, [2]Department of Geosciences, Princeton University, Princeton, NJ, USA, [3]Department of Earth and Environmental Sciences, University of Rochester, Rochester, NY, USA, [4]Scripps Institution of Oceanography, La Jolla, CA, USA

Key Points:
- Stable isotopes of nitrous oxide constrain marine versus terrestrial production 74,000–59,000 years ago
- Marine and terrestrial sources varied similarly across Dansgaard-Oeschger 19 and during the Marine Isotope Stage 5-4 transition
- Marine emissions dominated across Dansgaard-Oeschger 16/17; thus, abrupt N_2O increases were not all identical during the last glacial period

Supporting Information:
- Supporting Information S1

Correspondence to:
J. A. Menking,
james.menking@oregonstate.edu

Citation:
Menking, J. A., Brook, E. J., Schilt, A., Shackleton, S., Dyonisius, M., Severinghaus, J. P., et al. (2020). Millennial-scale changes in terrestrial and marine nitrous oxide emissions at the onset and termination of Marine Isotope Stage 4. *Geophysical Research Letters*, *47*, e2020GL089110. https://doi.org/10.1029/2020GL089110

Received 30 MAY 2020
Accepted 27 OCT 2020
Accepted article online 10 NOV 2020

Author Contributions:
Conceptualization: E. J. Brook, J. P. Severinghaus, V. V. Petrenko
Data curation: J. A. Menking, S. Shackleton
Formal analysis: J. A. Menking, A. Schilt
Investigation: J. A. Menking, S. Shackleton, M. Dyonisius
Methodology: A. Schilt
Resources: E. J. Brook, J. P. Severinghaus, V. V. Petrenko
Visualization: J. A. Menking, A. Schilt
Writing - original draft: J. A. Menking

Abstract Ice core measurements of the concentration and stable isotopic composition of atmospheric nitrous oxide (N_2O) 74,000–59,000 years ago constrain marine and terrestrial emissions. The data include two major Dansgaard-Oeschger (D-O) events and the N_2O decrease during global cooling at the Marine Isotope Stage (MIS) 5a-4 transition. The N_2O increase associated with D-O 19 (~73–71.5 ka) was driven by equal contributions from marine and terrestrial emissions. The N_2O decrease during the transition into MIS 4 (~71.5–67.5 ka) was caused by gradual reductions of similar magnitude in both marine and terrestrial sources. A 50 ppb increase in N_2O concentration at the end of MIS 4 was caused by gradual increases in marine and terrestrial emissions between ~64 and 61 ka, followed by an abrupt increase in marine emissions at the onset of D-O 16/17 (59.5 ka). This suggests that the importance of marine versus terrestrial emissions in controlling millennial-scale N_2O fluctuations varied in time.

Plain Language Summary Nitrous oxide is a powerful greenhouse gas that is produced naturally in soils and oceans. An important unresolved question is the extent to which anthropogenic warming will stimulate additional emissions from these sources, further adding to the warming. Past variations in the abundance of nitrous oxide have been observed using ice core reconstructions, but the reasons for the variations are not well understood. Nitrous oxide produced in soils is isotopically distinct from nitrous oxide produced in oceans. New measurements of the isotopes of atmospheric nitrous oxide provide constraints on how marine and terrestrial sources must have changed, driving fluctuations in nitrous oxide concentration during two intervals of rapid warming and a prolonged period of global cooling. The reconstructed changes in nitrous oxide sources provide insights into relationships between marine and terrestrial ecosystems and climate.

1. Introduction

Nitrous oxide is a long-lived greenhouse gas that also plays a role in the chemistry of the stratosphere. Ice core records show that N_2O varied on glacial-interglacial timescales over the last 800 ka (Schilt, Baumgartner, Blunier, et al., 2010; Spahni et al., 2005). The variations are closely coupled to climate cycles; N_2O concentration reached as high as 270 ppb during warm, interglacial periods and as low as 200 ppb during cold, glacial periods. High-resolution ice core records also show millennial-scale N_2O variability associated with glacial-interglacial transitions as well as the abrupt climate changes that occurred during the last glacial period (i.e., the Dansgaard-Oeschger [D-O] events) (Flückiger et al., 1999, 2004; Schilt, Baumgartner, Blunier, et al., 2010; Schilt, Baumgartner, Schwander, et al., 2010; Schilt et al., 2013; Sowers, 2001; Sowers et al., 2003).

It is thought that past N_2O variations were caused by changes in production rates in marine and terrestrial systems, where N_2O is a byproduct of microbial nitrification and denitrification (Stein & Yung, 2003). Marine N_2O production constitutes approximately 35% of modern emissions (Intergovernmental Panel on Climate Change, 2013; Kim & Craig, 1993) with open-ocean nitrification being the dominant production pathway (Battaglia & Joos, 2018; Freing et al., 2012; Nevison et al., 2003). "Hot spots" of denitrification have been identified in suboxic regions, such as the Arabian Sea, the subtropical North Pacific, the eastern tropical South Pacific, and coastal upwelling systems (Bange et al., 2001; Dore et al., 1998; Farias et al., 2009;

Naqvi et al., 2010), though estimates place the contribution of denitrification to modern marine N_2O emissions at a modest 4.5% (Battaglia & Joos, 2018). Other low-oxygen microbial pathways have recently been recognized, namely, anaerobic ammonium oxidation (anammox) and nitrifier denitrification (Zhu et al., 2013). While the exact mechanisms driving past N_2O variations on glacial-interglacial and millennial timescales are unknown, the sensitivity of marine nitrification and denitrification pathways to decreases in dissolved oxygen concentrations (e.g., Ji et al., 2018) has led many to hypothesize that marine oxygenation was the main control (e.g., Galbraith et al., 2008, 2013; Ganeshram et al., 2000; Schmittner et al., 2007; Schmittner & Galbraith, 2008).

Terrestrial N_2O production accounts for approximately 60% of the modern N_2O budget (Butterbach-Bahl et al., 2013; Intergovernmental Panel on Climate Change, 2013). There is evidence that denitrification is the more important N_2O production pathway in terrestrial environments (Vilain et al., 2014), though there is great spatiotemporal variability in both the mechanisms and magnitudes of N_2O production (Butterbach-Bahl et al., 2013). Temperature and soil moisture are the primary influences governing N_2O production in terrestrial environments (Bouwman et al., 1993; Xu et al., 2012). Additionally, a strong feedback exists between soil respiration rates and soil oxygenation, which in turn may influence denitrification rates (Butterbach-Bahl et al., 2013).

Ice core records of N_2O and CH_4 across rapid warming events show similarities in the timing of changes. CH_4 changes are highly correlated to terrestrial hydrology proxies and were likely caused by shifts in the latitudinal position of the tropical rain belts (Rhodes et al., 2015; Wang et al., 2001). The close correlation with N_2O has led some to hypothesize that terrestrial sources must have been responsible for the abrupt N_2O shifts in the past (e.g., Flückiger et al., 1999; Schilt et al., 2013). Past N_2O variations also show similarities with CO_2 (Flückiger et al., 2004; Schilt et al., 2013), which changed more gradually and often led increases in CH_4 by up to several thousand years (Ahn & Brook, 2008). The latter observation has fueled speculation that a significant component of N_2O variability is controlled by changes in marine emissions (Flückiger et al., 2004).

N_2O is removed from the atmosphere via photochemical destruction in the stratosphere. A recent modeling study suggested that the atmospheric lifetime of N_2O during the preindustrial period was 123 years (Prather et al., 2015), which also describes the *e*-folding time of a response to an instantaneous change in emissions. Modeling studies have shown that past changes in the atmospheric residence time were too small to significantly impact N_2O concentration (Crutzen & Bruhl, 1993; Martinerie et al., 1995; Murray et al., 2014); thus, the changes observed in the ice core record were driven by changes in N_2O emissions strength. N_2O is mixed in the atmosphere on timescales that are fast relative to its atmospheric lifetime.

Isotope studies of modern N_2O emissions suggest distinct differences in $\delta^{15}N$ and $\delta^{18}O$ of N_2O emitted from marine versus terrestrial ecosystems, so the isotopic composition of tropospheric N_2O provides a means of distinguishing the relative contribution of marine and terrestrial sources to the total atmospheric budget (Stein & Yung, 2003). Marine $\delta^{15}N$-N_2O ranges from 4‰ to 12‰ relative to air-N_2, with $\delta^{18}O$-N_2O ranging from 42‰ to 67‰ relative to VSMOW; terrestrial $\delta^{15}N$-N_2O ranges from −34‰ to 2‰, with $\delta^{18}O$-N_2O ranging from 20‰ to 43‰ (Kim & Craig, 1993; Rahn & Wahlen, 2000).

This study expands on the limited number of ice core N_2O studies by investigating the atmospheric history of N_2O and its isotopic composition between 74 and 59 ka. The interval includes two abrupt warming events (onset of D-O 19 at 72.2 ka and D-O 16/17 at 59.5 ka), the decrease in N_2O concentration associated with the Marine Isotope Stage (MIS) 5-4 transition (~71.5–67.5 ka), and a period of cold temperatures and ice sheet expansion (MIS 4). These large-scale climate shifts make this period interesting for studying the relationship between N_2O cycling and climate, and this study is complimentary to previous work that largely focused on the last deglaciation and the ongoing warm period (Fischer et al., 2019; Schilt et al., 2014). The new isotope data are used to determine plausible marine versus terrestrial source contributions to the variations in the total N_2O budget.

2. Materials and Methods

2.1. Large-Volume Ice Samples From Taylor Glacier

Taylor Glacier is an outlet glacier of the East Antarctic Ice Sheet that terminates in Taylor Valley in the McMurdo Dry Valleys. Old ice ranging in age from 7 to 150 ka outcrops in various places at the surface of

the glacier's ~80 km-long ablation zone (Aciego et al., 2007; Baggenstos et al., 2017; Kavanaugh et al., 2009; Shackleton et al., 2020). The archive has been utilized previously for gas isotope studies because it provides relatively easy access to large-volume ice samples (both in terms of drilling shallow cores and accessing the field site) (e.g., Bauska et al., 2016, 2018; Dyonisius et al., 2020; Petrenko et al., 2017; Schilt et al., 2014; Shackleton et al., 2020).

A new 19.8 m ice core was retrieved adjacent to the Taylor Glacier MIS 5-4 drill site, a location in which a complete archive of the MIS 5-4 transition was found in the gas and ice phases (Menking et al., 2019). The stratigraphy at this site is horizontal (isochrones in horizontal orientation with age increasing with depth), in contrast to nearby sites in which the stratigraphy is nearly vertical (Baggenstos et al., 2017). The new ice core was retrieved using the Blue Ice Drill (BID), a 24 cm diameter drill designed for retrieving shallow, large-volume ice cores (Kuhl et al., 2014). The core is referred to as the "MIS 5-4 BID3 core," as it is now the third large-diameter ice core retrieved from this site. The ~1 m core sections between 2 and 19.8 m depth were cut into quarter wedges in the field and stored at below −20°C on the glacier, in McMurdo Station, and en route to the laboratory freezer at Oregon State University (OSU).

2.2. CH_4 Measurements and Gas Chronology

CH_4 concentration was measured over the full length of the core by continuous flow analysis at OSU, following methods described by Rhodes et al. (2013) (Figure S1 in the supporting information). Sticks approximately 2.5 cm × 2.5 cm × 1 m were cut from the ¼ BID wedges retrieved from the field. The ice sticks were melted such that the outer bubble/water mixture was discarded, and the innermost melt stream was sampled. Air was separated from melt water in a gas permeable membrane, dried in a Nafion tube, and introduced continuously into a Picarro laser spectrometer that measures CH_4 abundance relative to air standards on the National Oceanic and Atmospheric Administration (NOAA04) methane concentration scale (Dlugokencky et al., 2005). Smoothing of the CH_4 signal due to dispersion and mixing of the gas stream during extraction and analysis (e.g., Rhodes et al., 2013; Stowasser et al., 2012) was minimal relative to the variations used to establish the chronology. Treatments to the raw CH_4 data are described in the supporting information.

The continuous CH_4 record for the MIS 5-4 BID3 core was used to develop the gas age chronology, as it captured background CH_4 variability that could be matched to preexisting ice core records. Tie points matching depth in the 5-4 BID3 core to age on the Antarctic ice core chronology 2012 (AICC2012) (Veres et al., 2013) were picked manually, similar to the approach used by Menking et al. (2019). CH_4 variations were matched to the EPICA Dronning Maud Land (EDML) CH_4 record (Schilt, Baumgartner, Schwander, et al., 2010) and show agreement with other Antarctic ice core CH_4 records as well as variations in Greenland temperature and isotope records from Hulu Cave speleothems (Figure S2). The timing of the local CH_4 maximum associated with D-O 18 (65 ka) is younger by 0.7 ka in the North Greenland Ice Core Project (NGRIP) core relative to the Taylor Glacier MIS 5-4 BID3 core, which is due to an inconsistency between the AICC2012 and GICC05 chronologies (Seierstad et al., 2014; Veres et al., 2013).

2.3. N_2O and N_2O Isotope Measurements

The BID wedges were cut in the OSU ice core freezer into 25 cm-long pieces. These were subsequently cut lengthwise to produce two depth adjacent (hence same aged) N_2O isotope samples for each 25 cm-depth interval. Samples were measured for $\delta^{15}N\text{-}N_2O$ and $\delta^{18}O\text{-}N_2O$ at OSU using a continuous flow gas chromatography-isotope ratio mass spectrometry technique originally described by Schilt et al. (2014). The N_2O bulk isotopic composition ($\delta^{15}N\text{-}N_2O$ and $\delta^{18}O\text{-}N_2O$) was measured using a Thermo MAT 253 mass spectrometer in continuous flow mode. The N_2O concentration of the air extracted from ice samples was determined from the ratio of the mass/charge 44 peak area and the amount of air in the extracted sample. Raw delta values and N_2O concentration values were calibrated by measuring standard air of determined isotopic composition and N_2O concentration (Table S1 and Figure S3). Details of the measurement procedure and calibration can be found in the supporting information.

Samples from 41 discrete depths were measured for N_2O concentration, $\delta^{15}N\text{-}N_2O$, and $\delta^{18}O\text{-}N_2O$ following the procedures described above, including six samples measured in replicate. The 1σ precisions were 1.28 ppb for N_2O concentration, 0.09‰ for $\delta^{15}N\text{-}N_2O$, and 0.88‰ for $\delta^{18}O\text{-}N_2O$. Replicate measurements

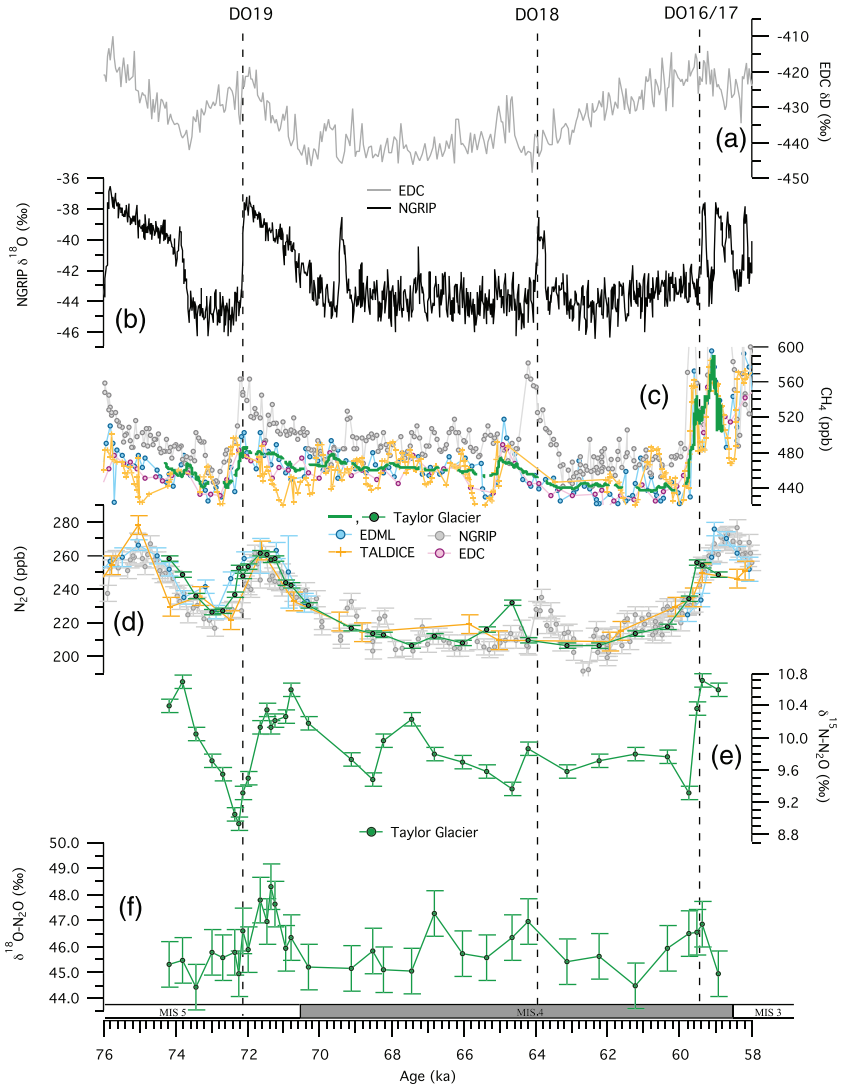

Figure 1. Taylor Glacier N_2O and N_2O isotope data spanning 74–59 ka. Water isotope records from EDC (a) and NGRIP (b) ice cores are shown for chronological reference (Andersen et al., 2004; Jouzel et al., 2007). All new data from Taylor Glacier are plotted in green (panels c–f). N_2O and CH_4 concentration records match preexisting data (c and d). There is a small offset in the timing of CH_4 and N_2O variations associated with D-O 18 (~64 ka) between the NGRIP and the EDML cores (and other Antarctic ice cores) despite both records being optimized to the AICC 2012 (Bazin et al., 2013). The vertical dashed lines indicate the abrupt Northern Hemisphere warming events D-O 19, D-O 18, and D-O 16/17 as represented in the NGRIP water isotope record.

were also made on archived samples dating to the last deglaciation, which showed good agreement with the published data (Schilt et al., 2014) (Figure S4).

3. Results

3.1. N_2O and N_2O Isotope Reconstructions

The new isotope record is the first data set of its kind to span the MIS 5-4 and MIS 4-3 transitions. The record captures N_2O concentration and stable isotope changes associated with Northern Hemisphere warming at the onset of D-O 19 (72.2 ka), as well as variations during the MIS 5-4 transition (Figure 1). The record also fully spans MIS 4 and part of the MIS 4-3 transition including the N_2O rise associated with the onset of D-O 16/17 (59.5 ka).

The excellent precision achieved during the measurement campaign allows interpretation of large and small features in the N_2O concentration record using the isotope history (Figure 1). The most outstanding features in the isotope records are the changes during the N_2O rise across D-O 19 (~73–71.5 ka). N_2O increased by 35 ppb while the $\delta^{15}N\text{-}N_2O$ first became lighter by 0.65‰, then more enriched by 1.45‰. The N_2O isotopic composition stabilized at the time of maximum N_2O concentration during D-O 19 (71.5 ka). As N_2O gradually dropped at the end of D-O 19 (corresponding to the MIS 5-4 transition), $\delta^{15}N\text{-}N_2O$ and $\delta^{18}O\text{-}N_2O$ decreased to more depleted values similar to before D-O 19. The precision of the $\delta^{18}O\text{-}N_2O$ measurement is poorer than for $\delta^{15}N\text{-}N_2O$, but it also resolves an enrichment trend between 73 and 71.5 ka.

Smaller variations in N_2O concentration and its isotopic composition occurred during MIS 4 between 69 and 62 ka. While N_2O concentration remained relatively low, there were oscillations in $\delta^{15}N\text{-}N_2O$ of up to 0.8‰ (Figure 1). Variations in $\delta^{18}O\text{-}N_2O$ are more difficult to discern given the lower precision of the measurement. Interestingly, N_2O increased by ~25 ppb at 64.5 ka, though the high N_2O concentration is only resolved by one data point. The N_2O increase may be associated with an N_2O excursion that is synchronous with abrupt warming at D-O 18, as observed in the NGRIP ice core (Schilt et al., 2013) (Figure 1), though the limited data resolution makes it difficult to rule out the possibility that the data point was influenced by an artifact due to some form of contamination. The age inconsistency between NGRIP and Antarctic ice cores does not affect our interpretations.

The youngest part of the record reproduces the large rise in N_2O concentration at the onset of the D-O 16/17 warming (59.5 ka) observed in other ice cores. During the N_2O rise, $\delta^{15}N\text{-}N_2O$ first decreased by 0.44‰, then increased by 1.4‰. Unfortunately, the feature is resolved by only a few data points, the latter two of which occur in the top 4 m of the core where thermal cracks in the glacier surface may affect the atmospheric archive (Baggenstos et al., 2017). While the transition to more enriched $\delta^{15}N\text{-}N_2O$ at 59.5 ka appears robust and synchronous with the rapid N_2O rise, the lack of resolution prohibits a more detailed interpretation of the MIS 4-3 transition.

The magnitudes of variations in the new $\delta^{15}N\text{-}N_2O$ and $\delta^{18}O\text{-}N_2O$ data are similar to variations observed during the deglaciation, though on average the new $\delta^{15}N\text{-}N_2O$ values are 0.4‰ lower than deglacial values (Fischer et al., 2019; Schilt et al., 2014) (Figure S5). No preexisting N_2O isotope data are available for comparison for the 74,000–59,000 year B.P. period. N_2O concentration, on the other hand, has been explored in detail in Greenlandic and Antarctic ice cores (e.g., Schilt, Baumgartner, Blunier, et al., 2010; Schilt, Baumgartner, Schwander, et al., 2010; Schilt et al., 2013). The new N_2O concentration record generally agrees well with the published data (Figure 1).

3.2. Source Histories

The N_2O and $\delta^{15}N\text{-}N_2O$ records were used to reconstruct marine and terrestrial source histories following methods described by Schilt et al. (2014) and recently used by Fischer et al. (2019). An inverse Monte Carlo approach was used to calculate 500 plausible marine and terrestrial source histories (Figure 2). $\delta^{18}O\text{-}N_2O$ data were not used to calculate source histories because of the larger measurement error. Splines were fit to N_2O and $\delta^{15}N\text{-}N_2O$ records, and a 1σ uncertainty band was generated with a Monte Carlo method. The oldest three data points were excluded from the spline fits because they do not resolve a full N_2O transition (Figure 1). The youngest two data points were also excluded because they are in the top 4 m of the ice core where thermal cracks may have caused contamination of air bubbles with modern air. A box model was solved inversely to determine the fraction of marine versus terrestrial emissions to the total N_2O source at model time = 0 (73 ka, fourth oldest data point in the new record). The model has tropospheric and stratospheric boxes (Figure S6) and simulates the addition of N_2O to the troposphere from terrestrial and marine N_2O sources (Schilt et al., 2014). The model also includes N_2O destruction in the stratosphere with a fixed ^{15}N fractionation factor (assuming a constant tropospheric lifetime for N_2O) (Table S2). To estimate uncertainties in the model results, a Monte Carlo method was employed to vary the model parameters, including the isotopic composition of marine and terrestrial sources, chosen randomly within their published uncertainties and/or range of natural variation (Table S2). Further details of the analysis are described in the supporting information.

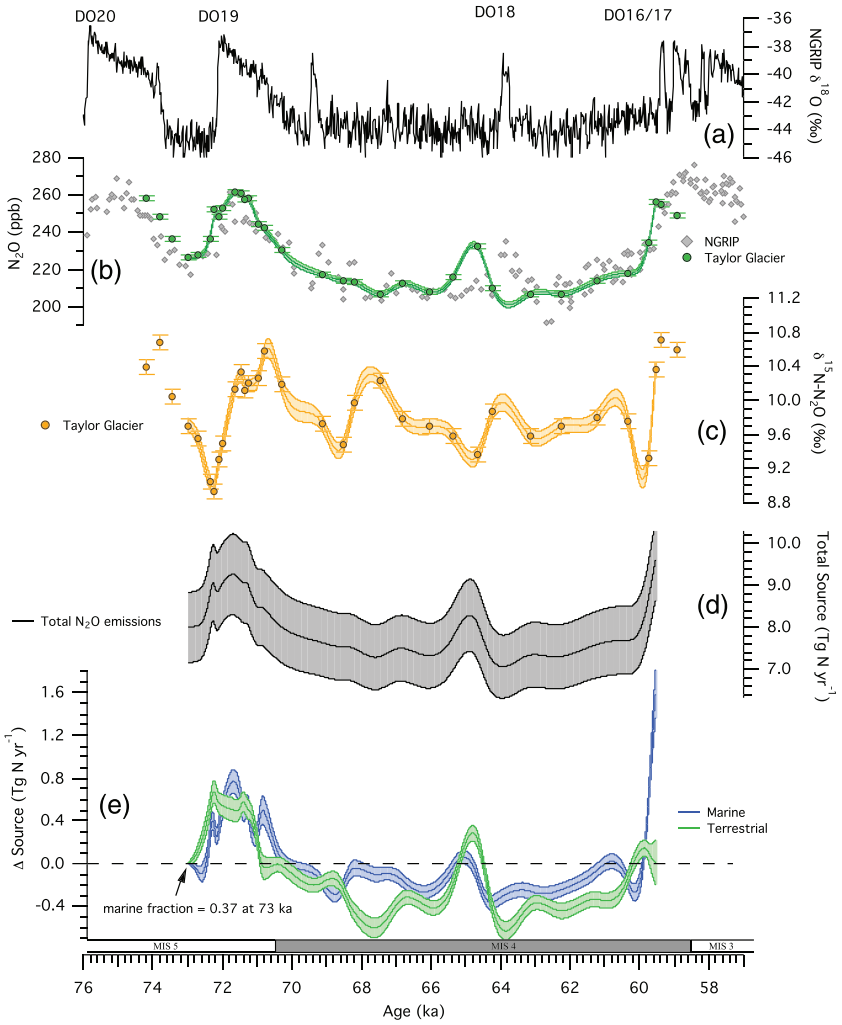

Figure 2. The mean and 1 standard deviation of 500 source histories for the period 73–59.5 ka. (a) The NGRIP water isotope record is plotted for chronological reference (Andersen et al., 2004). The source histories were determined by solving an inverse model constrained by splines fit to new N_2O concentration (b) and $\delta^{15}N\text{-}N_2O$ data (c) from Taylor Glacier. The changes in total N_2O source (d) as well as marine and terrestrial sources (blue and green lines, respectively) are plotted with their uncertainty bands (e). Uncertainties were calculated as the standard deviation of the 500 solutions at each time step after subtracting the absolute source magnitude from the initial value. The marine N_2O source was set to 37% at 73 ka (see text). Other source histories with different initial marine fractions show similar evolutions in time, though with different absolute values (Figure S7). Splines were fit to the new N_2O and $\delta^{15}N\text{-}N_2O$ records excluding the oldest four data points and the youngest two data points (see text). Repeating the inverse calculations without the data exclusions returned similar source histories (Figure S9).

The large ranges in published isotopic compositions for marine and terrestrial N_2O sources preclude the determination of the absolute marine versus terrestrial source fractions. To determine the change in emissions of the two sources, we assumed that the initial (73 ka) marine fraction was 37%, consistent with the modern preindustrial value (Intergovernmental Panel on Climate Change, 2013) and identical to the assumption of Schilt et al. (2014). This assumption is supported by the fact that the tropospheric $\delta^{15}N\text{-}N_2O$ at 73 ka (9.7‰) was similar to that of the preindustrial value (Bernard et al., 2006). The procedure described above — fitting splines to randomly perturbed data, randomly choosing a set of model parameters, and inversely solving the model for the marine fraction — was repeated until an initial marine fraction of 37% was obtained. The evolution of the marine fraction through time was then determined by solving the model inversely such that source changes reproduced the splines of N_2O concentration and $\delta^{15}N\text{-}N_2O$, assuming the isotopic ratios of the sources and other parameters remained constant through time.

To test the sensitivity of the solution to different assumptions of the initial marine fraction, source histories were also calculated where the initial marine fraction was 17% and 74% to bracket the full plausible range (Intergovernmental Panel on Climate Change, 2013). The source histories show similar evolutions for different initial marine fractions, implying that the changes in terrestrial and marine sources relative to each other do not depend significantly on the starting value (Figure S7). The 17% and 37% scenarios are similar in showing approximately equal increases in terrestrial and marine N_2O production during the N_2O rise across D-O 19 (73–71.5 ka). All solutions also exhibit a large increase in the marine source at the end of MIS 4 (onset of D-O 16/17, 59.5 ka) with relatively little contribution from the terrestrial source (Figure S7). Of the three scenarios, we consider the 74% case the least likely because the values required for $\delta^{15}N\text{-}N_2O$ of terrestrial emissions, $\delta^{15}N\text{-}N_2O$ of marine emissions, and stratospheric fractionation factor were on the extreme end of the published ranges (Figure S8). All of the major features of the determined source histories were robust despite choosing to exclude the oldest and youngest data points from the analysis (Figure S9).

Due to the strong isotopic fractionation during photochemical removal of N_2O in the stratosphere (Rockmann et al., 2001), increases or decreases in the total N_2O source can induce atmospheric disequilibria that result in short-lived changes in the tropospheric N_2O isotope ratio without any concomitant change in the overall isotopic composition of the N_2O source (i.e., marine and terrestrial fractions remain constant) (Tans, 1997). In order to estimate the magnitude of atmospheric disequilibrium, we used a forward model to calculate the tropospheric N_2O and $\delta^{15}N\text{-}N_2O$ response to the total emissions history that was determined using the inverse model described above but assuming constant fractions from marine and terrestrial emissions (constant source $\delta^{15}N\text{-}N_2O$). Disequilibrium effects cannot explain the full magnitude of the isotopic changes we observe (Figure S10). As a further check, we used the inverse model to determine the marine versus terrestrial source histories on the forward modeled N_2O and $\delta^{15}N\text{-}N_2O$. The model found solutions in which the relative fraction of marine emissions did not change significantly, suggesting that any disequilibrium effects contributing to the variations in our data are accounted for by the model inversion and represent a negligible fraction of the total suite of solutions.

In contrast to atmospheric CO_2, the effects of sea surface temperature changes on the N_2O concentration are minimal because the ocean reservoir of dissolved N_2O is relatively small. Therefore, the effect of solubility on N_2O concentration was ignored. There is also no observable temperature dependence of N_2O isotope fractionation during air-sea gas exchange of N_2O (Inoue & Mook, 1994), so the effects of sea surface temperature changes on N_2O isotopic composition were also neglected. These assumptions are similar to those made in previous studies (e.g., Fischer et al., 2019; Schilt et al., 2014).

4. Discussion

The features resolved in our new data set are of similar magnitude to variations in N_2O concentration and N_2O isotopes observed at the last deglaciation, during the last glacial period (Fischer et al., 2019; Schilt, Baumgartner, Schwander, et al., 2010; Schilt et al., 2014). We observe that the largest and fastest changes in N_2O concentration were concurrent with the abrupt CH_4 increases associated with the onset of D-O 19 (72.2 ka) and D-O 16/17 (59.5 ka). Smaller and more gradual increases in N_2O concentration appear to lead the CH_4 increases by up to 1–2 ka, similar to the phasing observed by others (Flückiger et al., 2004; Schilt, Baumgartner, Schwander, et al., 2010; Schilt et al., 2013). The largest changes in $\delta^{15}N\text{-}N_2O$ in the new data generally correspond to the largest N_2O concentration changes (Figure 1), implicating shifts in the isotopic composition of the total N_2O source. Given that these changes were generally associated with large-scale climate events, they likely resulted from significant changes in terrestrial hydrology and/or ocean circulation that changed the relative balance of marine versus terrestrial emissions. In the following sections, we discuss the major features of the new data in the context of the reconstructed source histories, and we speculate about the global environmental changes that may have been responsible for driving them.

4.1. N_2O Increase Across D-O 19 (73–71.5 Ka)

The abrupt warming at D-O 19 (72.2 ka) was associated with an increase in the total N_2O source from ~8.0 ± 0.8 to 9.3 ± 0.8 Tg N yr^{-1} (73–71.5 ka). This transition included similar increases in terrestrial and marine N_2O sources (Figure 2). Rapid environmental changes in terrestrial ecosystems have been documented on similar timescales. For example, speleothem records from low-latitude Chinese cave sites show large

variations in the Asian monsoon synchronous with D-O warming events (Wang et al., 2001, 2008). Rapid oscillations in $\delta^{18}O_{atm}$ observed in ice cores also show millennial-scale changes associated with D-O events, including at D-O 19, which reflect shifts in tropical hydrology that influenced the productivity of the terrestrial biosphere (Capron et al., 2012; Landais et al., 2007; Seltzer et al., 2017; Severinghaus et al., 2009). Other work highlights a strong feedback between soil N_2O production and the carbon cycle in response to warming (Butterbach-Bahl et al., 2013). Increased soil respiration rates driven by warmer temperatures cause lower soil oxygen levels. Coupled with increased nitrogen fixation, this may prime soils for increased N_2O production (Schaufler et al., 2010; Schindlbacher et al., 2004).

Other studies have explained the full magnitude of abrupt N_2O changes solely in terms of changes in marine N_2O production (e.g., Schmittner & Galbraith, 2008), with most work focusing on hypoxic "hot spots," where denitrification is highly sensitive to subsurface oxygen levels. Modern N_2O production is high in oxygen minimum zones such as the Arabian Sea, the Eastern Tropical North Pacific, the Indian Ocean, and the various low-latitude coastal upwelling regions (Bange et al., 1996, 2005; Dore et al., 1998). It has been proposed that Atlantic Meridional Overturning Circulation (AMOC) shifts occurred between cold Greenland stadials (weak AMOC) and warm interstadials (strong AMOC) (e.g., Henry et al., 2016; Pedro et al., 2018; Stocker & Johnsen, 2003), which forced variations in thermocline oxygenation in low- and high-latitude waters (Schmittner et al., 2007). In model simulations, weakened AMOC caused less nutrient delivery to low-latitude regions like the Indo-Pacific, the response to which was an increase in oxygen levels due to a lowering of phytoplankton productivity (because of less O_2 consumption during remineralization). At high latitudes, an increase in subsurface oxygen concentrations was due to increased mixed layer depth and steepened isopycnals (Schmittner et al., 2007). Support for this kind of AMOC mechanism may be found in millennial-scale fluctuations in denitrification rates documented in proxy records of sediment $\delta^{15}N$, organic carbon, and sediment color (Emmer & Thunell, 2000; Hendy et al., 2004; Ortiz et al., 2004; Schulz et al., 1998), as well as near-surface oxygen levels (Jaccard et al., 2014). Similar variations have also been demonstrated on glacial-interglacial timescales (Galbraith et al., 2008, 2013; Ganeshram et al., 2000).

Our data support a role for both marine and terrestrial N_2O emissions during the abrupt climate changes observed in the last glacial cycle, though it is important to note that D-O 19 is not necessarily representative of other D-O events. The only similarly abrupt increases in N_2O that are also characterized with N_2O stable isotope data are at the Bølling-Allerød warming (14.8 ka) (Schilt et al., 2014) and at D-O 16/17 (~59.5 ka) (this study). Box model inversions revealed equal magnitude changes in marine and terrestrial N_2O sources across the Bølling-Allerød (Figure S5) but with terrestrial sources changing significantly faster than marine sources (Fischer et al., 2019; Schilt et al., 2014). The variations at D-O 16/17 (59.5 ka) are discussed below.

4.2. N_2O Decrease During MIS 5-4 Transition and MIS 4

The total N_2O source decreased across the MIS 5a-4 transition (71.5–67.5 ka) with decreases in both marine and terrestrial sources contributing to the decline (Figure 2). The total N_2O source decreased by approximately 26% from the local maximum during D-O 19 (71.5 ka). Total N_2O emissions were not lower than 7.0 ± 0.9 Tg N yr^{-1} during MIS 4, approximately 77% the magnitude of the total preindustrial N_2O source. In general, the largest $\delta^{15}N\text{-}N_2O$ variations in the new data set correspond to intervals of largest N_2O concentration change; however, there is an exception to this during the MIS 5-4 transition in that $\delta^{15}N\text{-}N_2O$ oscillated between locally high and low values during the descent into MIS 4 (~71.5–67.5 ka) while N_2O gradually decreased. Indeed, a full $\delta^{15}N\text{-}N_2O$ excursion and recovery between 68.5 and 66 ka occurred while N_2O concentration was steadily low and global climate was cold. The implication is that the relative reductions in marine versus terrestrial sources contributing to that decrease were not steady. Shifts in terrestrial and marine production occurred despite relatively stable and cold climate.

Our reconstructed source histories suggest terrestrial sources may have decreased more during MIS 4 relative to marine sources, particularly at ~67 ka (Figure 2). It is somewhat surprising that decreases in marine N_2O emissions did not dominate the N_2O budget during this interval because the MIS 5-4 transition is recognized as a period of major ocean circulation reorganization characterized by a shoaling of NADW, filling of the deep Atlantic with Antarctic Bottom Water, and stratification of the deep ocean (Adkins, 2013; Thornalley et al., 2013). Such changes might reasonably be expected to lower N_2O emissions by decreasing

nutrient delivery to productive regions of the ocean, reducing O_2 consumption (Schmittner et al., 2007; Schmittner & Galbraith, 2008).

A hypothesis for why marine N_2O emissions did not decrease more is that while most N_2O-producing regions of the ocean experienced a prolonged period of weakened emissions, conditions in the Southern Ocean may have actually compensated N_2O production, or even increased it. The overall effect of increased Southern Ocean productivity due to iron fertilization (Anderson et al., 2014; Martinez-Garcia et al., 2014) may have been a reduction in thermocline O_2 that boosted (or at least lessened any decrease in) Southern Ocean N_2O emissions. Increased Southern Ocean sea ice extent (e.g., Wolff et al., 2006) also would have decreased surface water ventilation, contributing to subsurface O_2 decline. Enhanced stratification may have reduced O_2 levels, though this is also expected to reduce nutrient supply, decreasing primary productivity (Flückiger et al., 2004; Goldstein et al., 2003). Recent quantitative reconstructions of deep Pacific oxygen concentrations over the last 30 ka indicate widespread dysoxia or near-anoxia during the Last Glacial Maximum in conjunction with increased carbon storage (Anderson et al., 2019). MIS 4 also reflects a period of increased deep ocean carbon storage (Yu et al., 2016), with qualitative proxies demonstrating evidence for deep O_2 decline (Jaccard et al., 2016). Mixing of low-O_2 deep waters into the Southern Ocean thermocline therefore may have boosted N_2O outgassing. Measurements of dissolved N_2O in the modern ocean show a plume of deep water enriched in N_2O outcropping near Antarctica (Figure S11), reinforcing the notion that the Southern Ocean could have been a source of N_2O to the atmosphere in the past.

The later part of MIS 4 is characterized by a slow rise in N_2O concentration, in parallel with warming Antarctic temperatures, similar to that observed in the later part of stadials preceding D-O events (Flückiger et al., 2004), and in model simulations (Schmittner & Galbraith, 2008). The model simulations suggest this feature is due to the slow recovery of thermocline nutrient levels and primary productivity (and therefore slow decline of O_2) after a stadial AMOC collapse (Schmittner & Galbraith, 2008). It is possible this feature is of similar origin, though our reconstructions show slow increases in both terrestrial and marine sources between 64 and 61 ka, suggesting that the slow ramp-up of N_2O preceding D-O events may also have a land origin.

4.3. N_2O Increase at D-O 16/17 (59.5 ka)

The end of MIS 4 is marked by the largest feature in the reconstructed N_2O source history — total N_2O emissions increased by 1.8 ± 1.0 Tg N yr^{-1} between 60.2 and 59.5 ka, with the fastest N_2O jump closely associated with the onset of abrupt warming at D-O 16/17 (59.5 ka). Marine emissions almost solely explain the increase (Figure 2). It has been previously noted that larger N_2O increases tended to occur at the onsets of longer interstadials (Flückiger et al., 2004), which typically followed longer stadials during the last glacial period (Schmittner & Galbraith, 2008). Insofar as MIS 4 may be considered an especially prolonged and cold stadial, the N_2O change at D-O 16/17 is consistent with this observed relationship.

The dominance of marine N_2O emissions is in contrast to the more balanced N_2O emissions across D-O 19 (73–71.5 ka), implying that not all Northern Hemisphere warming events of the last glacial period were alike in terms of N_2O production in marine and terrestrial ecosystems. It is surprising that marine emissions dominated the N_2O rise at the onset of D-O 16/17 (59.5 ka) because this interval features the largest CH_4 concentration increase in the record. The latter observation indicates a change in the terrestrial hydrological cycle that stimulated CH_4 production (Rhodes et al., 2015), and one might reasonably expect this would impact terrestrial N_2O production similarly. A plausible explanation is that the regions of N_2O and CH_4 production on land were distinct.

The dominance of marine emissions at D-O 16/17 (59.5 ka) is different from the N_2O rise at the Bølling-Allerød warming, which was driven by equal increases in marine and terrestrial emissions (Fischer et al., 2019; Schilt et al., 2014) (Figure S5). The Bølling-Allerød event followed a prolonged cold stadial (the Last Glacial Maximum) and was concurrent with changes in AMOC (McManus et al., 2004), the terrestrial hydrologic cycle (Wang et al., 2001), and the terrestrial biosphere (Severinghaus et al., 2009), similar to MIS 4. One might then reasonably expect N_2O increases at D-O 16/17 were also equal parts marine and terrestrial. We suggest the difference between the two events was that the last deglaciation involved a much greater scale of global climate change than the termination of MIS 4, including larger changes in the extent of Northern Hemisphere ice sheets and terrestrial biogeochemical cycling (Clark et al., 2012).

The dominance of marine emissions at the onset of D-O 16/17 (59.5 ka) could be due to rapid reorganization of ocean water masses and a dramatic lowering of thermocline O_2 as AMOC resumed strength. Bulk sediment $\delta^{15}N$ records from the Equatorial Pacific suggest increases in denitrification across the MIS 4-3 transition (Robinson et al., 2007). The changes at the MIS 4-3 transition (and throughout the last 70 ka) are coherent with changes in Antarctic climate that point to an important role for Southern Ocean nutrient utilization for governing low-latitude thermocline O_2 (Robinson et al., 2007). The pathway for Southern Ocean preformed nutrients to feed the subsurface Pacific is the northward spreading of Subantarctic Mode Water (Sarmiento et al., 2004). The connection between Southern Ocean nutrient utilization and low-latitude denitrification rates is interesting given that large changes in CO_2 and depletion of $\delta^{13}C$-CO_2 occurred at this time (Eggleston et al., 2016). If the MIS 4-3 transition represents a dramatic weakening of the efficiency of the Southern Ocean biological pump and a return of remineralized nutrients (and ventilation of CO_2) from the deep, then this might represent a trigger for increases in low-latitude marine productivity that drove N_2O production.

The question remains why N_2O cycling was different at D-O 19 (73–71.5 ka) versus D-O 16/17 (59.5 ka). We suggest that the background climate state prior to the onset of the warming event is important for determining the potential strength of terrestrial and marine N_2O emissions. D-O 19 occurred after a shorter duration stadial and when ice sheets were relatively smaller. D-O 16/17 occurred after much colder and longer-duration glacial conditions, concurrent with large changes in carbon cycling that conspired to store CO_2 (and nutrients) in the deep ocean (Jaccard et al., 2016; Yu et al., 2016). We suggest this primed the marine ecosystem for greater marine N_2O production when AMOC resumed and potentially stifled production in soils.

5. Conclusions

New high-resolution N_2O isotope data provide constraints on the balance of terrestrial and marine N_2O sources at the beginning of the last glacial period. The records allow reconstructions of emission histories when N_2O concentration was changing across the MIS 5-4 transition (71.5–67.5 ka), D-O 19 (72.2–71.5 ka), MIS 4 (69.5–60 ka), and at the onset of D-O 16/17 (59.5 ka). Decreases in terrestrial and marine N_2O sources were approximately equally responsible for lowering atmospheric N_2O through most of MIS 4, however, marine emissions dominated the rapid N_2O increase observed at the MIS 4-3 transition (D-O 16/17). This is in contrast to the 35 ppb increase in N_2O concentration associated with the Northern Hemisphere warming at D-O 19, during which marine and terrestrial emissions contributed approximately equally. Our results imply that the response of N_2O production to abrupt warming during the last glacial period was not always identical. Rather, the relative strength of marine versus terrestrial emissions controlling abrupt N_2O increases appears to have changed through time.

Conflict of Interest

The authors declare no conflicts of interest.

Data Availability Statement

The data presented in this manuscript are available in the United States Antarctic Program Data Center (https://doi.org/10.15784/601398).

Acknowledgments

We thank Mike Jayred for drilling the ice core used for this study, especially on the "spur of the moment." We also thank Kathy Schroeder for managing the Taylor Glacier field camp. We thank Peter Sperlich, Isaac Vimont, Peter Neff, Heidi Roop, Bernhard Bereiter, Jake Ward, and Andrew Smith for their help with field logistics and drilling, sampling, and packing ice cores. We thank the United States Antarctic Program, with particular thanks to Science Cargo, the BFC, and Helicopter Operations. This research was supported by the National Science Foundation Office of Polar Programs (grant PLR-1245821, PLR-1245659, and PLR-1246148). We thank Mike Kaplan and one anonymous reviewer for their helpful feedback on the original draft of this manuscript.

References

Aciego, S. M., Cuffey, K. M., Kavanaugh, J. L., Morse, D. L., & Severinghaus, J. P. (2007). Pleistocene ice and paleo-strain rates at Taylor Glacier, Antarctica. *Quaternary Research*, *68*(3), 303–313. https://doi.org/10.1016/j.yqres.2007.07.013

Adkins, J. F. (2013). The role of deep ocean circulation in setting glacial climates. *Paleoceanography*, *28*, 539–561. https://doi.org/10.1002/palo.20046

Ahn, J., & Brook, E. J. (2008). Atmospheric CO_2 and climate on millennial time scales during the last glacial period. *Science*, *322*(5898), 83–85. https://doi.org/10.1126/science.1160832

Andersen, K. K., Azuma, N., Barnola, J. M., Bigler, M., Biscaye, P., Caillon, N., et al. (2004). High-resolution record of Northern Hemisphere climate extending into the last interglacial period. *Nature*, *431*(7005), 147–151. https://doi.org/10.1038/nature02805

Anderson, R. F., Barker, S., Fleisher, M., Gersonde, R., Goldstein, S. L., Kuhn, G., et al. (2014). Biological response to millennial variability of dust and nutrient supply in the Subantarctic South Atlantic Ocean. *Philosophical Transactions of the Royal Society a-Mathematical Physical and Engineering Sciences*, *372*(2019), 17. https://doi.org/10.1098/rsta.2013.0054

Anderson, R. F., Sachs, J. P., Fleisher, M. Q., Allen, K. A., Yu, J. M., Koutavas, A., & Jaccard, S. L. (2019). Deep-sea oxygen depletion and ocean carbon sequestration during the last ice age. *Global Biogeochemical Cycles*, *33*, 301–317. https://doi.org/10.1029/2018GB006049

Baggenstos, D., Bauska, T. K., Severinghaus, J. P., Lee, J. E., Schaefer, H., Buizert, C., et al. (2017). Atmospheric gas records from Taylor Glacier, Antarctica, reveal ancient ice with ages spanning the entire last glacial cycle. *Climate of the Past*, *13*(7), 943–958. https://doi.org/10.5194/cp-13-943-2017

Bange, H. W., Naqvi, S. W. A., & Codispoti, L. A. (2005). The nitrogen cycle in the Arabian Sea. *Progress in Oceanography*, *65*(2–4), 145–158. https://doi.org/10.1016/j.pocean.2005.03.002

Bange, H. W., Rapsomanikis, S., & Andreae, M. O. (1996). Nitrous oxide in coastal waters. *Global Biogeochemical Cycles*, *10*(1), 197–207. https://doi.org/10.1029/95GB03834

Bange, H. W., Rapsomanikis, S., & Andreae, M. O. (2001). Nitrous oxide cycling in the Arabian Sea. *Journal of Geophysical Research*, *106*(C1), 1053–1065. https://doi.org/10.1029/1999JC000284

Battaglia, G., & Joos, F. (2018). Marine N_2O emissions from nitrification and denitrification constrained by modern observations and projected in multimillennial global warming simulations. *Global Biogeochemical Cycles*, *32*, 92–121. https://doi.org/10.1002/2017GB005671

Bauska, T. K., Baggenstos, D., Brook, E. J., Mix, A. C., Marcott, S. A., Petrenko, V. V., et al. (2016). Carbon isotopes characterize rapid changes in atmospheric carbon dioxide during the last deglaciation. *Proceedings of the National Academy of Sciences of the United States of America*, *113*(13), 3465–3470. https://doi.org/10.1073/pnas.1513868113

Bauska, T. K., Brook, E. J., Marcott, S. A., Baggenstos, D., Shackleton, S., Severinghaus, J. P., & Petrenko, V. V. (2018). Controls on millennial-scale atmospheric CO_2 variability during the last glacial period. *Geophysical Research Letters*, *45*, 7731–7740. https://doi.org/10.1029/2018GL077881

Bazin, L., Landais, A., Lemieux-Dudon, B., Toyé Mahamadou Kele, H., Veres, D., Parrenin, F., et al. (2013). An optimized multi-proxy, multi-site Antarctic ice and gas orbital chronology (AICC2012): 120–800 ka. *Climate of the Past*, *9*(4), 1715–1731. https://doi.org/10.5194/cp-9-1715-2013

Bernard, S., Rockmann, T. R., Kaiser, J., Barnola, J. M., Fischer, H., Blunier, T., & Chappellaz, J. (2006). Constraints on N_2O budget changes since pre-industrial time from new firn air and ice core isotope measurements. *Atmospheric Chemistry and Physics*, *6*, 493–503.

Bouwman, A. F., Fung, I., Matthews, E., & John, J. (1993). Global analysis of the potential for N_2O production in natural soils. *Global Biogeochemical Cycles*, *7*(3), 557–597. https://doi.org/10.1029/93GB01186

Butterbach-Bahl, K., Baggs, E. M., Dannenmann, M., Kiese, R., & Zechmeister-Boltenstern, S. (2013). Nitrous oxide emissions from soils: How well do we understand the processes and their controls? *Philosophical Transactions of the Royal Society, B: Biological Sciences*, *368*(1621), 20130122. https://doi.org/10.1098/rstb.2013.0122

Capron, E., Landais, A., Chappellaz, J., Buiron, D., Fischer, H., Johnsen, S. J., et al. (2012). A global picture of the first abrupt climatic event occurring during the last glacial inception. *Geophysical Research Letters*, *39*, L15703. https://doi.org/10.1029/2012GL052656

Clark, P. U., Shakun, J. D., Baker, P. A., Bartlein, P. J., Brewer, S., Brook, E., et al. (2012). Global climate evolution during the last deglaciation. *Proceedings of the National Academy of Sciences of the United States of America*, *109*(19), E1134–E1142. https://doi.org/10.1073/pnas.1116619109

Crutzen, P. J., & Bruhl, C. (1993). A model study of atmospheric temperatures and the concentrations of ozone, hydroxyl, and some other photochemically active gases during the glacial, the preindustrial Holocene and the present. *Geophysical Research Letters*, *20*(11), 1047–1050. https://doi.org/10.1029/93GL01423

Dlugokencky, E. J., Myers, R. C., Lang, P. M., Masarie, K. A., Crotwell, A. M., Thoning, K. W., et al. (2005). Conversion of NOAA atmospheric dry air CH_4 mole fractions to a gravimetrically prepared standard scale. *Journal of Geophysical Research*, *110*, D18306. https://doi.org/10.1029/2005JD006035

Dore, J. E., Popp, B. N., Karl, D. M., & Sansone, F. J. (1998). A large source of atmospheric nitrous oxide from subtropical North Pacific surface waters. *Nature*, *396*(6706), 63–66. https://doi.org/10.1038/23921

Dyonisius, M. N., Petrenko, V. V., Smith, A. M., Hua, Q., Yang, B., Schmitt, J., et al. (2020). Old carbon reservoirs were not important in the deglacial methane budget. *Science*, *367*(6480), 907–910. https://doi.org/10.1126/science.aax0504

Eggleston, S., Schmitt, J., Bereiter, B., Schneider, R., & Fischer, H. (2016). Evolution of the stable carbon isotope composition of atmospheric CO_2 over the last glacial cycle. *Paleoceanography*, *31*, 434–452. https://doi.org/10.1002/2015PA002874

Emmer, E., & Thunell, R. C. (2000). Nitrogen isotope variations in Santa Barbara Basin sediments: Implications for denitrification in the eastern tropical North Pacific during the last 50,000 years. *Paleoceanography*, *15*(4), 377–387. https://doi.org/10.1029/1999PA000417

Farias, L., Castro-Gonzalez, M., Cornejo, M., Charpentier, J., Faundez, J., Boontanon, N., & Yoshida, N. (2009). Denitrification and nitrous oxide cycling within the upper oxycline of the eastern tropical South Pacific oxygen minimum zone. *Limnology and Oceanography*, *54*(1), 132–144. https://doi.org/10.4319/lo.2009.54.1.0132

Fischer, H., Schmitt, J., Bock, M., Seth, B., Joos, F., Spahni, R., et al. (2019). N_2O changes from the Last Glacial Maximum to the preindustrial—Part 1: Quantitative reconstruction of terrestrial and marine emissions using N2O stable isotopes in ice cores. *Biogeosciences*, *16*(20), 3997–4021. https://doi.org/10.5194/bg-16-3997-2019

Flückiger, J., Blunier, T., Stauffer, B., Chappellaz, J., Spahni, R., Kawamura, K., et al. (2004). N_2O and CH_4 variations during the last glacial epoch: Insight into global processes. *Global Biogeochemical Cycles*, *18*, GB1020. https://doi.org/10.1029/2003GB002122

Flückiger, J., Dallenbach, A., Blunier, T., Stauffer, B., Stocker, T. F., Raynaud, D., & Barnola, J. M. (1999). Variations in atmospheric N_2O concentration during abrupt climatic changes. *Science*, *285*(5425), 227–230. https://doi.org/10.1126/science.285.5425.227

Freing, A., Wallace, D. W. R., & Bange, H. W. (2012). Global oceanic production of nitrous oxide. *Philosophical Transactions of the Royal Society, B: Biological Sciences*, *367*(1593), 1245–1255. https://doi.org/10.1098/rstb.2011.0360

Galbraith, E. D., Kienast, M., Albuquerque, A. L., Altabet, M. A., Batista, F., Bianchi, D., et al. (2013). The acceleration of oceanic denitrification during deglacial warming. *Nature Geoscience*, *6*(7), 579–584. https://doi.org/10.1038/ngeo1832

Galbraith, E. D., Schmittner, A., & Jaccard, S. L. (2008). Abrupt increase of nitrous oxide production in the Indo-Pacific at the onset of the Bölling warm period. *Geochimica et Cosmochimica Acta*, *72*(12), A290–A290.

Ganeshram, R. S., Pedersen, T. F., Calvert, S. E., McNeill, G. W., & Fontugne, M. R. (2000). Glacial-interglacial variability in denitrification in the world's oceans: Causes and consequences. *Paleoceanography*, *15*(4), 361–376. https://doi.org/10.1029/1999PA000422

Goldstein, B., Joos, F., & Stocker, T. F. (2003). A modeling study of oceanic nitrous oxide during the Younger Dryas cold period. *Geophysical Research Letters*, *30*(2), 1092. https://doi.org/10.1029/2002GL016418

Hendy, I. L., Pedersen, T. F., Kennett, J. P., & Tada, R. (2004). Intermittent existence of a southern Californian upwelling cell during submillennial climate change of the last 60 kyr. *Paleoceanography*, *19*, PA3007. https://doi.org/10.1029/2003PA000965

Henry, L. G., McManus, J. F., Curry, W. B., Roberts, N. L., Piotrowski, A. M., & Keigwin, L. D. (2016). North Atlantic ocean circulation and abrupt climate change during the last glaciation. *Science*, *353*(6298), 470–474. https://doi.org/10.1126/science.aaf5529

Inoue, H. Y., & Mook, W. G. (1994). Equilibrium and kinetic nitrogen and oxygen-isotope fractionations between dissolved and gaseous N_2O. *Chemical Geology*, *113*(1–2), 135–148. https://doi.org/10.1016/0009-2541(94)90009-4

Intergovernmental Panel on Climate Change (2013). Working Group 1 Contribution to the IPCC Fifth Assessment Report on Climate Change 2013: The Physical Science Basis*Rep*.

Jaccard, S. L., Galbraith, E. D., Frolicher, T. L., & Gruber, N. (2014). Ocean (de)oxygenation across the last deglaciation: Insights for the future. *Oceanography*, *27*(1), 26–35.

Jaccard, S. L., Galbraith, E. D., Martinez-Garcia, A., & Anderson, R. F. (2016). Covariation of deep Southern Ocean oxygenation and atmospheric CO_2 through the last ice age. *Nature*, *530*(7589), 207–210. https://doi.org/10.1038/nature16514

Ji, Q. X., Buitenhuis, E., Suntharalingam, P., Sarmiento, J. L., & Ward, B. B. (2018). Global nitrous oxide production determined by oxygen sensitivity of nitrification and denitrification. *Global Biogeochemical Cycles*, *32*, 1790–1802. https://doi.org/10.1029/2018GB005887

Jouzel, J., Masson-Delmotte, V., Cattani, O., Dreyfus, G., Falourd, S., Hoffmann, G., et al. (2007). Orbital and millennial Antarctic climate variability over the past 800,000 years. *Science*, *317*(5839), 793–796. https://doi.org/10.1126/science.1141038

Kavanaugh, J. L., Cuffey, K. M., Morse, D. L., Conway, H., & Rignot, E. (2009). Dynamics and mass balance of Taylor Glacier, Antarctica: 1. Geometry and surface velocities. *Journal of Geophysical Research*, *114*, F04010. https://doi.org/10.1029/2009JF001309

Kim, K. R., & Craig, H. (1993). N-15 and O-18 characteristics of nitrous oxide—A global perspective. *Science*, *262*(5141), 1855–1857. https://doi.org/10.1126/science.262.5141.1855

Kuhl, T. W., Johnson, J. A., Shturmakov, A. J., Goetz, J. J., Gibson, C. J., & Lebar, D. A. (2014). A new large-diameter ice-core drill: The Blue Ice Drill. *Annals of Glaciology*, *55*(68), 1–6. https://doi.org/10.3189/2014AoG68A009

Landais, A., Masson-Delmotte, V., Nebout, N. C., Jouzel, J., Blunier, T., Leuenberger, M., et al. (2007). Millennial scale variations of the isotopic composition of atmospheric oxygen over Marine Isotopic Stage 4. *Earth and Planetary Science Letters*, *258*(1–2), 101–113. https://doi.org/10.1016/j.epsl.2007.03.027

Martinerie, P., Brasseur, G. P., & Granier, C. (1995). The chemical composition of ancient atmospheres—A model study constrained by ice core data. *Journal of Geophysical Research*, *100*(D7), 14,291–14,304. https://doi.org/10.1029/95JD00826

Martinez-Garcia, A., Sigman, D. M., Ren, H. J., Anderson, R. F., Straub, M., Hodell, D. A., et al. (2014). Iron fertilization of the Subantarctic Ocean during the last ice age. *Science*, *343*(6177), 1347–1350. https://doi.org/10.1126/science.1246848

McManus, J. F., Francois, R., Gherardi, J. M., Keigwin, L. D., & Brown-Leger, S. (2004). Collapse and rapid resumption of Atlantic meridional circulation linked to deglacial climate changes. *Nature*, *428*(6985), 834–837. https://doi.org/10.1038/nature02494

Menking, J. A., Brook, E. J., Shackleton, S. A., Severinghaus, J. P., Dyonisius, M. N., Petrenko, V., et al. (2019). Spatial pattern of accumulation at Taylor Dome during Marine Isotope Stage 4: Stratigraphic constraints from Taylor Glacier. *Climate of the Past*, *15*(4), 1537–1556. https://doi.org/10.5194/cp-15-1537-2019

Murray, L. T., Mickley, L. J., Kaplan, J. O., Sofen, E. D., Pfeiffer, M., & Alexander, B. (2014). Factors controlling variability in the oxidative capacity of the troposphere since the Last Glacial Maximum. *Atmospheric Chemistry and Physics*, *14*(7), 3589–3622. https://doi.org/10.5194/acp-14-3589-2014

Naqvi, S. W. A., Bange, H. W., Farias, L., Monteiro, P. M. S., Scranton, M. I., & Zhang, J. (2010). Marine hypoxia/anoxia as a source of CH_4 and N_2O. *Biogeosciences*, *7*(7), 2159–2190. https://doi.org/10.5194/bg-7-2159-2010

Nevison, C., Butler, J. H., & Elkins, J. W. (2003). Global distribution of N_2O and the ΔN_2O-AOU yield in the subsurface ocean. *Global Biogeochemical Cycles*, *17*(4), 1119. https://doi.org/10.1029/2003GB002068

Ortiz, J. D., O'Connell, S. B., DelViscio, J., Dean, W., Carriquiry, J. D., et al. (2004). Enhanced marine productivity off western North America during warm climate intervals of the past 52 ky. *Geology*, *32*(6), 521–524. https://doi.org/10.1130/g20234.1

Pedro, J. B., Jochum, M., Buizert, C., He, F., Barker, S., & Rasmussen, S. O. (2018). Beyond the bipolar seesaw: Toward a process understanding of interhemispheric coupling. *Quaternary Science Reviews*, *192*, 27–46. https://doi.org/10.1016/j.quascirev.2018.05.005

Petrenko, V. V., Smith, A. M., Schaefer, H., Riedel, K., Brook, E., Baggenstos, D., et al. (2017). Minimal geological methane emissions during the Younger Dryas–Preboreal abrupt warming event. *Nature*, *548*(7668), 443–446. https://doi.org/10.1038/nature23316

Prather, M. J., Hsu, J., DeLuca, N., Jackman, C. H., Oman, L. D., Douglass, A. R., et al. (2015). Measuring and modeling the lifetime of nitrous oxide including its variability. *Journal of Geophysical Research: Atmospheres*, *120*, 5693–5705. https://doi.org/10.1002/2015JD023267

Rahn, T., & Wahlen, M. (2000). A reassessment of the global isotopic budget of atmospheric nitrous oxide. *Global Biogeochemical Cycles*, *14*(2), 537–543. https://doi.org/10.1029/1999GB900070

Rhodes, R. H., Brook, E. J., Chiang, J. C. H., Blunier, T., Maselli, O. J., McConnell, J. R., et al. (2015). Enhanced tropical methane production in response to iceberg discharge in the North Atlantic. *Science*, *348*(6238), 1016–1019. https://doi.org/10.1126/science.1262005

Rhodes, R. H., Fain, X., Stowasser, C., Blunier, T., Chappellaz, J., McConnell, J. R., et al. (2013). Continuous methane measurements from a late Holocene Greenland ice core: Atmospheric and in-situ signals. *Earth and Planetary Science Letters*, *368*, 9–19. https://doi.org/10.1016/j.epsl.2013.02.034

Robinson, R. S., Mix, A., & Martinez, P. (2007). Southern Ocean control on the extent of denitrification in the southeast Pacific over the last 70 ka. *Quaternary Science Reviews*, *26*(1–2), 201–212. https://doi.org/10.1016/j.quascirev.2006.08.005

Rockmann, T., Kaiser, J., Brenninkmeijer, C. A. M., Crowley, J. N., Borchers, R., Brand, W. A., & Crutzen, P. J. (2001). Isotopic enrichment of nitrous oxide ((NNO)-N-15-N-14, (NNO)-N-14-N-15, (NNO)-N-14-N-14-O-18) in the stratosphere and in the laboratory. *Journal of Geophysical Research*, *106*(D10), 10,403–10,410. https://doi.org/10.1029/2000JD900822

Sarmiento, J. L., Gruber, N., Brzezinski, M. A., & Dunne, J. P. (2004). High-latitude controls of thermocline nutrients and low latitude biological productivity. *Nature*, *427*(6969), 56–60. https://doi.org/10.1038/nature02127

Schaufler, G., Kitzler, B., Schindlbacher, A., Skiba, U., Sutton, M. A., & Zechmeister-Boltenstern, S. (2010). Greenhouse gas emissions from European soils under different land use: Effects of soil moisture and temperature. *European Journal of Soil Science*, *61*(5), 683–696. https://doi.org/10.1111/1.1365-2389.2010.01277.x

Schilt, A., Baumgartner, M., Blunier, T., Schwander, J., Spahni, R., Fischer, H., & Stocker, T. F. (2010). Glacial-interglacial and millennial-scale variations in the atmospheric nitrous oxide concentration during the last 800,000 years. *Quaternary Science Reviews*, *29*(1–2), 182–192. https://doi.org/10.1016/j.quascirev.2009.03.011

Schilt, A., Baumgartner, M., Eicher, O., Chappellaz, J., Schwander, J., Fischer, H., & Stocker, T. F. (2013). The response of atmospheric nitrous oxide to climate variations during the last glacial period. *Geophysical Research Letters*, *40*, 1888–1893. https://doi.org/10.1002/grl.50380

Schilt, A., Baumgartner, M., Schwander, J., Buiron, D., Capron, E., Chappellaz, J., et al. (2010). Atmospheric nitrous oxide during the last 140,000 years. *Earth and Planetary Science Letters*, *300*(1–2), 33–43. https://doi.org/10.1016/j.epsl.2010.09.027

Schilt, A., Brook, E. J., Bauska, T. K., Baggenstos, D., Fischer, H., Joos, F., et al. (2014). Isotopic constraints on marine and terrestrial N_2O emissions during the last deglaciation. *Nature*, *516*(7530), 234–237. https://doi.org/10.1038/nature13971

Schindlbacher, A., Zechmeister-Boltenstern, S., & Butterbach-Bahl, K. (2004). Effects of soil moisture and temperature on NO, NO_2, and N_2O emissions from European forest soils. *Journal of Geophysical Research*, *109*, D17302. https://doi.org/10.1029/2004JD004590

Schmittner, A., & Galbraith, E. D. (2008). Glacial greenhouse-gas fluctuations controlled by ocean circulation changes. *Nature*, *456*(7220), 373–376. https://doi.org/10.1038/nature07531

Schmittner, A., Galbraith, E. D., Hostetler, S. W., Pedersen, T. F., & Zhang, R. (2007). Large fluctuations of dissolved oxygen in the Indian and Pacific oceans during Dansgaard-Oeschger oscillations caused by variations of North Atlantic Deep Water subduction. *Paleoceanography*, *22*, PA3207. https://doi.org/10.1029/2006PA001384

Schulz, H., von Rad, U., & Erlenkeuser, H. (1998). Correlation between Arabian Sea and Greenland climate oscillations of the past 110,000 years. *Nature*, *393*(6680), 54–57.

Seierstad, I. K., Abbott, P. M., Bigler, M., Blunier, T., Bourne, A. J., Brook, E., et al. (2014). Consistently dated records from the Greenland GRIP, GISP2 and NGRIP ice cores for the past 104 ka reveal regional millennial-scale $\delta^{18}O$ gradients with possible Heinrich event imprint. *Quaternary Science Reviews*, *106*, 29–46. https://doi.org/10.1016/j.quascirev.2014.10.032

Seltzer, A. M., Buizert, C., Baggenstos, D., Brook, E. J., Ahn, J., Yang, J. W., & Severinghaus, J. P. (2017). Does $\delta^{18}O$ of O_2 record meridional shifts in tropical rainfall? *Climate of the Past*, *13*(10), 1323–1338. https://doi.org/10.5194/cp-13-1323-2017

Severinghaus, J. P., Beaudette, R., Headly, M. A., Taylor, K., & Brook, E. J. (2009). Oxygen-18 of O_2 records the impact of abrupt climate change on the terrestrial biosphere. *Science*, *324*(5933), 1431–1434. https://doi.org/10.1126/science.1169473

Shackleton, S., Baggenstos, D., Menking, J. A., Dyonisius, M. N., Bereiter, B., Bauska, T. K., et al. (2020). Global ocean heat content in the Last Interglacial. *Nature Geoscience*, *13*(1), 77–81. https://doi.org/10.1038/s41561-019-0498-0

Sowers, T. (2001). N_2O record spanning the penultimate deglaciation from the Vostok ice core. *Journal of Geophysical Research*, *106*(D23), 31,903–31,914. https://doi.org/10.1029/2000JD900707

Sowers, T., Alley, R. B., & Jubenville, J. (2003). Ice core records of atmospheric N_2O covering the last 106,000 years. *Science*, *301*(5635), 945–948. https://doi.org/10.1126/science.1085293

Spahni, R., Chappellaz, J., Stocker, T. F., Loulergue, L., Hausammann, G., Kawamura, K., et al. (2005). Atmospheric methane and nitrous oxide of the late Pleistocene from Antarctic ice cores. *Science*, *310*(5752), 1317–1321. https://doi.org/10.1126/science.1120132

Stein, L. Y., & Yung, Y. L. (2003). Production, isotopic composition, and atmospheric fate of biologically produced nitrous oxide. *Annual Review of Earth and Planetary Sciences*, *31*, 329–356. https://doi.org/10.1146/annurev.earth.31.110502.080901

Stocker, T. F., & Johnsen, S. J. (2003). A minimum thermodynamic model for the bipolar seesaw. *Paleoceanography*, *18*(4), 1087. https://doi.org/10.1029/2003PA000920

Stowasser, C., Buizert, C., Gkinis, V., Chappellaz, J., Schüpbach, S., Bigler, M., et al. (2012). Continuous measurements of methane mixing ratios from ice cores. *Atmospheric Measurement Techniques*, *5*(5), 999–1013. https://doi.org/10.5194/amt-5-999-2012

Tans, P. P. (1997). A note on isotopic ratios and the global atmospheric methane budget. *Global Biogeochemical Cycles*, *11*(1), 77–81. https://doi.org/10.1029/96GB03940

Thornalley, D. J. R., Barker, S., Becker, J., Hall, I. R., & Knorr, G. (2013). Abrupt changes in deep Atlantic circulation during the transition to full glacial conditions. *Paleoceanography*, *28*, 253–262. https://doi.org/10.1002/palo.20025

Veres, D., Bazin, L., Landais, A., Toyé Mahamadou Kele, H., Lemieux-Dudon, B., Parrenin, F., et al. (2013). The Antarctic ice core chronology (AICC2012): An optimized multi-parameter and multi-site dating approach for the last 120 thousand years. *Climate of the Past*, *9*(4), 1733–1748. https://doi.org/10.5194/cp-9-1733-2013

Vilain, G., Garnier, J., Decuq, C., & Lugnot, M. (2014). Nitrous oxide production from soil experiments: Denitrification prevails over nitrification. *Nutrient Cycling in Agroecosystems*, *98*(2), 169–186. https://doi.org/10.1007/s10705-014-9604-2

Wang, Y. J., Cheng, H., Edwards, R. L., An, Z. S., Wu, J. Y., Shen, C. C., & Dorale, J. A. (2001). A high-resolution absolute-dated Late Pleistocene monsoon record from Hulu Cave, China. *Science*, *294*(5550), 2345–2348. https://doi.org/10.1126/science.1064618

Wang, Y. J., Cheng, H., Edwards, R. L., Kong, X. G., Shao, X. H., Chen, S. T., et al. (2008). Millennial- and orbital-scale changes in the East Asian monsoon over the past 224,000 years. *Nature*, *451*(7182), 1090–1093. https://doi.org/10.1038/nature06692

Wolff, E. W., Fischer, H., Fundel, F., Ruth, U., Twarloh, B., Littot, G. C., et al. (2006). Southern Ocean sea-ice extent, productivity and iron flux over the past eight glacial cycles. *Nature*, *440*(7083), 491–496. https://doi.org/10.1038/nature04614

Xu, R., Prentice, I. C., Spahni, R., & Niu, H. S. (2012). Modelling terrestrial nitrous oxide emissions and implications for climate feedback. *The New Phytologist*, *196*(2), 472–488. https://doi.org/10.1111/j.1469-8137.2012.04269.x

Yu, J., Menviel, L., Jin, Z. D., Thornalley, D. J. R., Barker, S., Marino, G., et al. (2016). Sequestration of carbon in the deep Atlantic during the last glaciation. *Nature Geoscience*, *9*(4), 319–324. https://doi.org/10.1038/ngeo2657

Zhu, X., Burger, M., Doane, T. A., & Horwath, W. R. (2013). Ammonia oxidation pathways and nitrifier denitrification are significant sources of N_2O and NO under low oxygen availability. *Proceedings of the National Academy of Sciences of the United States of America*, *110*(16), 6328–6333. https://doi.org/10.1073/pnas.1219993110